

# ERMES

Wolfgang Plastino<sup>a,b</sup>, Matthias Laubenstein<sup>c</sup>,  
Giuseppe Etiope<sup>d</sup>, Paolo Favali<sup>d</sup>

<sup>a</sup> Department of Physics, University of Roma Tre,  
via della Vasca Navale, 84, I-00146, Rome (Italy)

<sup>b</sup> National Institute for Nuclear Physics, Section Rome III,  
via della Vasca Navale, 84, I-00146, Rome (Italy)

<sup>c</sup> National Institute for Nuclear Physics, Underground Laboratories of Gran Sasso,  
S.S.17bis km 18+910, I-67010, Assergi (AQ) (Italy)

<sup>d</sup> National Institute for Geophysics and Volcanology, RIDGE unit  
Roma 2 Department, via di Vigna Murata, 605, I-00143, Rome (Italy)

## Abstract

The Environmental Radioactivity Monitoring for Earth Sciences (ERMES) research project has the following topics: a) correlations between the variations of radon with the strain processes of the rock [1],[2],[3] and transport properties related to the groundwater geochemistry [4]; b) radiocarbon and tritium high precision liquid scintillation spectrometry [5]; c) new devices development for nuclear spectrometry analyzing the light-yield properties of different scintillator crystals under extreme physical-chemical environmental conditions for geophysical prospecting and investigations for the volcanology, seismology and oceanography [6]. In this report we show the preliminary environmental radioactivity analysis on sea-water samples collected by GEOSTAR deep-sea observatory. The data seem to point out a mixing of water mass characterizing the dynamic interface between lithosphere (seabed) and ocean (sea-water).

## 1 Introduction

The Benthic Boundary Layer (BBL) is the dynamic interface between lithosphere (seabed) and ocean (sea-water) where many physical, geochemical and biological processes occur playing an important role in environmental global changes. Geohazards, carbon cycle, heat flow, life generation, climatic oceanography, are only some examples of local or global processes whose comprehension is today limited due to the lack of data related to the deep ocean floors. Lithospheric processes at the BBL impact the marine environment at different temporal and spatial scales. Earthquakes produce short-term effects (landslides and tsunamis) that threaten the lives and economy of coastal communities, while outgassing of greenhouse gases and mineral-rich fluids impact long-term global climates

and the formation of economically important mineral resources. The BBL has an important role on carbon cycle being either a potentially sinking or transition zone for carbon coming from shallower zones or from the lithosphere. Oil platforms are sited on the BBL, and cables and pipelines are laid across it. Delicate marine ecosystems have evolved in these extreme environment, yet it may be significantly affected by man's activities. The BBL dynamics however is not completely clear: it is not known how it is perturbed by energy and mass release from the seabed (seismicity, heat flow, gas diffusion, biological productivity, diagenetic reactions), what distances the particles and waves can be transported, what is the evolution and fate of bottom currents and storms. In this framework, the environmental radioactivity monitoring is a useful tool to better understand the BBL physical processes and its dynamics.

## 2 Experimental setup

GEOSTAR-2 (GEophysical and Oceanographic STation for Abyssal Research) is the first European deep-sea observatory for geophysical and environmental monitoring at seabed becoming operative in 2000. It was deployed in September 2000 from the Italian oceanographic ship *Urania*, in the southern Tyrrhenian Sea, between the Sicilian coast and the island of Ustica, at a depth of about 2000 m. This area was chosen as pilot test site being a key area for the Tyrrhenian seismicity and oceanography. After 206 days, in April 2001, the observatory was recovered. The sensors used for this mission (2 magnetometers, a prototype gravity meter, a hydrophone, a Doppler currentmeter, a single-point currentmeter, an automatic water sampler for laboratory geochemical analysis, a CTD and a transmissometer) were continuously controlled and managed by a data acquisition and control system able to transmit the data via surface buoy and radio or satellite link to on-shore operators. This mission represented the longest lasting experiment using a complex module, with an intelligent unit, deployed at great depths. The environmental radioactivity measurements of the sea-water samples collected by GEOSTAR have been performed by High Purity Germanium (HPGe) coaxial detectors with characteristics summarized in Figures 1 and 2.

Each sea-water sample has been measured for about ten days using polyethylene box of 70 mm diameter and 30 mm height.

## 3 Results and Discussion

The spectrum of one sea-water sample is shown in Figure 3.

The environmental radioactivity analysis of the sea-water samples collected by GEOSTAR is shown in Figure 4.

In this preliminary step, the data seem to emphasize that GEOSTAR was able to observe environmental changes in the benthic boundary sea-water due to the interaction of lithosphere with a water mass moving vertically. This hypothesis may be confirmed by geochemical tracers as helium isotopes. These analyses are carrying out and seem to justify this sea-water mixing also with the temperature and Doppler currentmeter data.

## 4 Conclusions

The physical properties of the BBL and its dynamics may be analyzed by multiparametric approach only. In this framework, the environmental radioactivity analysis of sea-water samples has a particular interest because it emphasizes, particularly, the mixing of water mass with different origin and better constrains the physical sources for the BBL dynamical processes. Then, the deep-sea observation and monitoring systems developed in the last decade, such as GEOSTAR, can contribute to cover a scientific gap on the oceanography physical of BBL.

**Acknowledgments** The authors wish to dedicate this work to Dr. Giuseppe Smriglio unexpectedly died during this research activity. The authors are grateful to Prof. Alessandro Bettini for the his kind collaboration and Mr. Massimiliano De Deo of the LNGS for the useful and precious assistance.

## References

- [1] Plastino, W. et. al., Laboratori Nazionali del Gran Sasso, Annual Report from 1997 to 2001.
- [2] Plastino, W. and Bella, F., 2001, *Radon groundwater monitoring at underground laboratories of Gran Sasso (Italy)*, Geophysical Research Letters, 28 (14), 2675-2678.
- [3] Plastino, W., Bella, F., Catalano, P.G. and Di Giovambattista, R., 2002, *Radon groundwater anomalies related to the Umbria-Marche September 26, 1997 earthquakes*, Geofisica Internacional, 41(4), 369-375.
- [4] Caputo, M. and Plastino, W., 2003, *Diffusion with space memory*, in "Geodesy, the challenge of the 3rd millenium", eds.: Grafarend, E., Krumm, F. and Schwarze, V., Springer Verlag, Berlin-Heidelberg, 429-435.
- [5] Plastino, W., Kaihola, L., Bartolomei, P. and Bella, F., 2001, *Cosmic background reduction in the radiocarbon measurements by liquid scintillation spectrometry at the underground laboratory of Gran Sasso*, Radiocarbon, 43 (2A), 157-161.
- [6] Plastino, W., De Felice, P. and de Notaristefani, F., 2002, *Radon gamma-ray spectrometry with YAP:Ce scintillator*, Nuclear Instruments and Methods in Physics Research, A, 486/1-2, 146-149.

| Detector      | volume [cm <sup>3</sup> ] | Relative efficiency | FWHM* [keV] |
|---------------|---------------------------|---------------------|-------------|
| GePV p-type   | 225                       | 56%                 | 2.0         |
| GeCris p-type | 468                       | 120%                | 2.0         |
| GsOr p-type   | 414                       | 96%                 | 1.9         |

\* FWHM of the *full energy peak* at 1332.47 keV for <sup>60</sup>Co.

Figure 1: Table. 1. Characteristics of the HPGe coaxial detectors.

| Detector | Total background and for several radionuclides (counts/days) |                             |                             |                            |
|----------|--|-----------------------------|-----------------------------|----------------------------|
|          | (60–2700) keV  | <sup>214</sup> Bi (352 keV) | <sup>208</sup> Tl (583 keV) | <sup>40</sup> K (1461 keV) |
| GePV     | 951  | 5.3                         | 4.1                         | 6.3                        |
| GeCris   | 221  | 1.2                         | 0.2                         | 3.4                        |
| GsOr     | 980  | 5.1                         | 1.7                         | 8.4                        |

Figure 2: Table. 2. Background of the HPGe coaxial detectors.

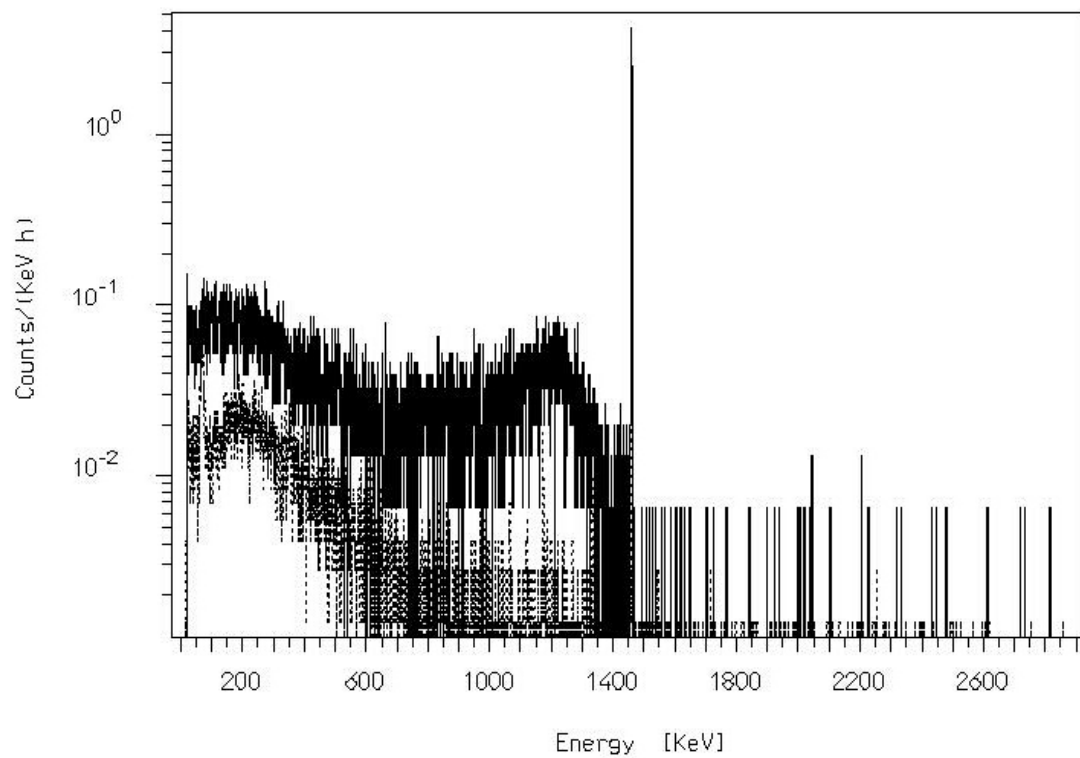


Figure 3: fig. 1. The spectrum of the sample n. 6 (solid line). The background of the HPGe (GeCris) detector is also showed (dashed line).

| Sampl. | mass | <sup>226</sup> Ra | <sup>234</sup> Pa | <sup>235</sup> U | <sup>228</sup> Ra | <sup>228</sup> Th | <sup>40</sup> K | <sup>137</sup> Cs | <sup>60</sup> Co |
|--------|------|-------------------|-------------------|------------------|-------------------|-------------------|-----------------|-------------------|------------------|
|        | g    | mBq/kg            | mBq/kg            | mBq/kg           | mBq/kg            | mBq/kg            | Bq/kg           | mBq/kg            | mBq/kg           |
| 1      | 87,6 | < 1,43E+1         | < 1,07E+3         | < 9,10E+0        | < 2,15E+1         | < 1,10E+1         | 12.8±1.3        | 8.1±4.1           | < 9,40E+0        |
| 2      | 86,5 | < 1,54E+1         | < 1,09E+3         | < 9,60E+0        | < 2,43E+1         | < 1,12E+1         | 13.2±1.3        | < 6,50E+0         | < 6,60E+0        |
| 3      | 62,5 | < 3,05E+1         | < 1,44E+3         | < 2,01E+1        | < 4,08E+1         | < 3,57E+1         | 9.3±1.4         | < 9,80E+0         | < 1,12E+1        |
| 4      | 62,6 | < 1,38E+1         | < 8,94E+2         | < 9,20E+0        | < 2,21E+1         | < 1,12E+1         | 12.7±1.3        | 9.6±3.9           | < 6,20E+0        |
| 5      | 88,1 | < 2,23E+1         | < 1,48E+3         | < 1,68E+1        | < 2,79E+1         | < 2,65E+1         | 11.3±1.6        | < 7,20E+0         | < 8,10E+0        |
| 6      | 80,2 | < 1,43E+1         | < 1,10E+3         | < 9,50E+0        | < 2,39E+1         | < 1,21E+1         | 12.6±1.3        | < 6,30E+0         | < 7,30E+0        |
| 7      | 80,2 | < 2,81E+1         | < 1,81E+3         | < 1,90E+1        | < 3,73E+1         | < 3,45E+1         | 10.9±1.6        | < 9,50E+0         | < 1,09E+1        |
| 8      | 80,8 | < 1,36E+1         | < 1,11E+3         | < 8,60E+0        | < 2,23E+1         | < 1,06E+1         | 12.5±1.3        | < 5,80E+0         | < 6,30E+0        |
| 9      | 80,5 | < 2,82E+1         | < 1,94E+3         | < 1,99E+1        | < 4,27E+1         | < 3,53E+1         | 11.7±1.7        | < 1,00E+1         | < 1,08E+1        |
| 10     | 82,0 | < 1,57E+1         | < 1,24E+3         | < 9,40E+0        | < 2,42E+1         | < 1,54E+1         | 12.7±1.3        | < 7,00E+0         | < 7,60E+0        |
| 11     | 80,9 | < 2,41E+1         | < 1,33E+3         | < 1,38E+1        | < 3,16E+1         | < 2,66E+1         | 11.3±1.6        | < 1,08E+1         | < 8,80E+0        |
| 12     | 81,8 | < 2,05E+1         | < 1,05E+3         | < 1,23E+1        | < 2,59E+1         | < 3,19E+1         | 10.8±1.5        | < 9,10E+0         | < 7,10E+0        |
| 13     | 82,5 | < 2,56E+1         | < 1,51E+3         | < 1,62E+1        | < 3,36E+1         | < 2,93E+1         | 10.8±1.5        | < 8,30E+0         | < 9,00E+0        |
| 14     | 89,0 | < 1,25E+1         | < 9,55E+2         | < 8,20E+0        | < 1,96E+1         | < 9,70E+0         | 12.5±1.3        | 8.0±3.6           | < 5,70E+0        |
| 15     | 89,3 | < 2,15E+1         | < 1,48E+3         | < 1,53E+1        | < 2,85E+1         | < 2,76E+1         | 11.3±1.5        | < 7,20E+0         | < 8,60E+0        |
| 16     | 89,5 | 27.3±19.9         | < 7,00E+2         | < 9,40E+0        | < 1,64E+1         | < 1,74E+1         | 11.5±1.6        | < 6,40E+0         | < 5,10E+0        |
| 17     | 60,9 | < 3,19E+1         | < 1,40E+3         | < 1,97E+1        | < 4,13E+1         | < 3,74E+1         | 10.0±1.5        | < 9,80E+0         | < 1,13E+1        |
| 18     | 57,5 | < 1,65E+1         | < 1,24E+3         | < 1,13E+1        | < 2,89E+1         | < 1,75E+1         | 13.2±1.4        | < 7,40E+0         | < 8,20E+0        |
| 19     | 60,9 | < 2,90E+1         | < 1,18E+3         | < 1,84E+1        | < 3,70E+1         | < 3,55E+1         | 10.7±1.5        | < 9,50E+0         | < 1,07E+1        |
| 20     | 57,5 | < 1,55E+1         | < 1,18E+3         | < 1,01E+1        | < 2,57E+1         | < 1,35E+1         | 13.2±1.4        | < 6,40E+0         | < 7,00E+0        |
| 21     | 65,8 | < 2,37E+1         | < 9,89E+2         | < 1,38E+1        | < 3,04E+1         | < 2,91E+1         | 10.9±1.5        | 13.9±6.7          | < 8,00E+0        |
| 22     | 62,5 | < 2,11E+1         | < 1,13E+3         | < 1,38E+1        | < 3,73E+1         | < 2,17E+1         | 12.4±0.4        | < 9,70E+0         | < 1,18E+1        |
| 23     | 63,4 | < 2,10E+1         | < 1,19E+3         | < 1,36E+1        | < 3,20E+1         | < 2,07E+1         | 12.7±0.4        | < 1,01E+1         | < 1,24E+1        |

GeCris

GePV

GsOr

GeMPI

Figure 4: Table. 3. Environmental Radioactivity analysis of the sea-water samples collected by GEOSTAR